International Journal of Nanomedicine

Dovepress
open access to scientific and medical research

Open Access Full Text Article

ORIGINAL RESEARCH

HucMSC-Exo Induced N2 Polarization of Neutrophils: Implications for Angiogenesis and Tissue Restoration in Wound Healing

Jiaman Yang[1,2,*], Yulin Xie[1,2,*], Zhikuan Xia[1,*], Shuaifei Ji[3,*], Xin Yang[1], Danxia Yue[1], Yuanyuan Liu[1,3], Rongya Yang[1–3], Yunlong Fan[1,3]

[1]Department of Dermatology, the Seventh Medical Center of Chinese PLA General Hospital, Beijing, 100700, People's Republic of China; [2]The Second School of Clinical Medicine, SouThern Medical University, Guangzhou, 510599, People's Republic of China; [3]Chinese PLA Medical School, Beijing, 100853, People's Republic of China

*These authors contributed equally to this work

Correspondence: Rongya Yang, Department of Dermatology, the Seventh Medical Center of Chinese PLA General Hospital, No. 5, Nanmencang Alley, Dongsi Shitiao, Dongcheng District, Beijing, 100700, People's Republic of China, Email YangRY301hospital@163.com; Yunlong Fan, Department of Dermatology, the Seventh Medical Center of Chinese PLA General Hospital, No. 5, Nanmencang alley, Dongsi Shitiao, Dongcheng District, Beijing, 100700, People's Republic of China, Email FanYL301hospital@163.com

Background: Neutrophils rapidly accumulate in large numbers at sites of tissue damage, exhibiting not only their well-known bactericidal capabilities but also playing crucial roles in angiogenesis and tissue repair. While exosomes derived from human umbilical cord mesenchymal stem cells (HucMSC-Exo) have emerged as a promising therapeutic tool, their exact mechanisms of action remain partly elusive. We hypothesize that HucMSC-Exo treatment may modulate neutrophil phenotypes, thereby significantly influencing wound healing outcomes.

Methods: HucMSC-Exo were isolated via ultracentrifugation and subsequently administered through subcutaneous injection into full-thickness cutaneous wounds in mice. To determine the impact of host neutrophils on the healing effects of HucMSC-Exo in skin injuries, strategies including neutrophil depletion and adoptive transfer were employed. Flow cytometry was used to evaluate the proportion of N2 subtype neutrophils in both normal and diabetic wounds, and the effect of HucMSC-Exo on this proportion was assessed. Furthermore, the mitochondrial metabolic reprogramming driven by HucMSC-Exo during N2 polarization was investigated through JC1 staining, ATP quantification, fatty acid uptake assays, and assessment of FAO-related genes (*Cpt1b, Acadm, and Acadl*).

Results: Depleting host neutrophils strikingly dampened prohealing effect of HucMSC-Exo on skin injury, while adoptive transfer of bone marrow neutrophils rescued this process. During normal healing process, some neutrophils expressed N2 markers, in contrast, diabetic wounds exhibited a reduced expression of N2 markers. After treatment with HucMSC-Exo, most neutrophils increased the phosphorylation of STAT6, leading to mitochondrial metabolic reprogramming and thus acquired an N2 phenotype. These N2 neutrophils, polarized by HucMSC-Exo, boosted the release of proangiogenic factors, particularly BV8, a myeloid cell-derived proangiogenic factor, and induced angiogenesis thereby favoring tissue restoration.

Conclusion: This research uniquely demonstrates the identification of N2 neutrophils in skin injury and shows that HucMSC-Exo could skew neutrophils toward N2 phenotype, enhancing our insight into how cells react to HucMSC-Exo.

Keywords: HucMSC-Exo, neutrophils, phenotype switching, cutaneous wound healing, tissue restoration

Introduction

Exosomes derived from human umbilical cord mesenchymal stem cells (HucMSC-Exo) have emerged as a promising tool in regeneration medicine, offering potential benefits for facilitating wound healing.[1–3] While there is existing evidence supporting the idea that HucMSC-Exo promotes wound healing, there is a lack of consistent reporting on the molecular mechanisms involving diverse cell populations.[4,5] This inconsistency may result from the cellular diversity involved in healing and the complexities of the immune system within wounds.

Received: 14 February 2024
Accepted: 10 April 2024
Published: 13 April 2024

Graphical Abstract

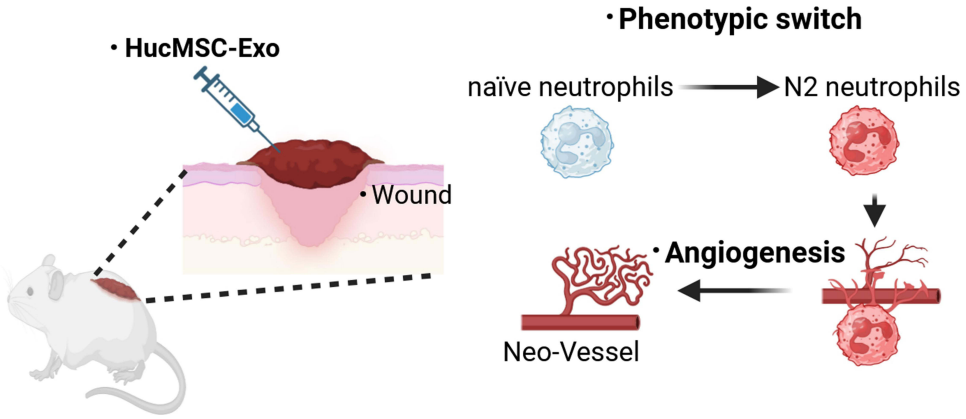

Cutaneous wound repair is a complex and interconnected process involving various cells that act in coordination to manage inflammation, proliferation, and remodeling.[6] Transitioning from the early inflammation to subsequent proliferation stages is a pivotal point for healing outcomes.[7] Among the immune cells involved in wound healing, neutrophils are the first to be recruited and dominate in numbers during the early stages after injury.[8] If the skin barrier is breached, neutrophils play a crucial role in limiting bacterial translocation. Activated neutrophils degranulate, releasing proteases and coordinating the healing response. Following their demise through NETosis, neutrophils release chromatin and form neutrophil extracellular traps to trap pathogens.[9] Despite these potent functions, these activities of neutrophils can lead to collateral damage, contributing to excess inflammation and hinder tissue repair, leading to a somewhat negative perception of neutrophils in the context of tissue restoration. Nevertheless, recent studies indicate a need to reassess the conventional perspective on neutrophils.[8,10]

Over the past decade, there has been significant exploration of phenotypic heterogeneity in macrophages.[11–13] The current consensus is that macrophages transition from an inflammatory M1 state right after injury to an anti-inflammatory M2 state, assisting in inflammation resolution and tissue healing.[13,14] In contrast to macrophages, the phenotypic heterogeneity of neutrophils has been understudied, partly due to their short lifespan (only 10 hours in circulation) and nonadherent nature in culture.[15]

The objective of this research was to investigate how myeloid cells, especially neutrophils, contribute to the healing-promoting impact of HucMSC-Exo at the wound site. Previously, we characterized the heterogeneity of neutrophils and macrophages during HucMSC-Exo-mediated tissue repair through single-cell sequencing.[16] Herein, we found that the pro-healing effect of HucMSC-Exo heavily depended on infiltrated neutrophils rather than macrophages. Adding complexity to this, HucMSC-Exo guided the phenotypic switching of neutrophils at the wound site, directly reprogramming naïve neutrophils (N0) into an anti-inflammatory proangiogenetic status (N2). The reprogrammed N2 neutrophils exhibited the capability to produce angiogenic factors, such as vascular endothelial growth factor (VEGF) proteins and BV8. Further investigation into the signaling pathway revealed that STAT6 signaling played a critical role in the metabolic regulation of N2 polarization during HucMSC-Exo stimulation. By impacting mitochondrial metabolism, HucMSC-Exo induced metabolic reprogramming messages that converged upon fatty acid oxidation (FAO), lipid metabolism, and mitochondrial adaptations, consequently driving neutrophils into another immunometabolic cell fate.

Methods

Cell Culture and Reagents

The SVEC4-10 mouse endothelial cell line and the HL-60 human neutrophilic promyelocyte cell line were both sourced from the American Type Culture Collection and cultivated in their appropriate media—RPMI-1640 or DMEM—

supplemented with 10% fetal bovine serum, streptomycin (100 mg/mL), and penicillin (100 units/mL). For the isolation of mouse primary neutrophils from C57BL/6N mice, femur and tibia were extracted from euthanized mice. A 25-gauge needle filled with 1× Hanks's balanced salt solution (HBSS) 0.38% sodium citrate buffer was used to flush the bones. The extracted cell suspension was gently disintegrated and filtered through a 40 μm Corning cell strainer to obtain a single cell suspension. Red blood cells were removed using Servicebio's (Wuhan, China) red blood cell lysis buffer, with a hypotonic lysis step included. After washing in HBSS, neutrophils were further purified via a Miltenyi Biotec magnetic associated cell sorting (MACS)-based protocol (kit# 130–097-658), then maintained in RPMI-1640. All cell cultures were kept at 37°C with 5% CO2.

Hucmsc-Exo Isolation and Identification

HucMSC-Exo were offered by Aiyi Life Technology Co., Ltd. The producer cells were cultured under serum-free conditions in DMEM medium for 48 hours, and the supernatant was collected for exosome isolation by a sequence of centrifugation steps at 1000×g for 10 minutes, 4000×g for 20 minutes, and 10,000×g for 40 minutes, followed by ultracentrifugation at 100,000×g for 70 minutes at 4°C.[17] The resulting solution was resuspended in PBS and filtered through a 0.22 μm filter.

Nanoparticle tracking analysis (NTA) with a Nanosizer™ measured the size distribution of the HucMSC-Exo. Their morphology was assessed via transmission electron microscopy (TEM) while Western blotting probed for the surface markers CD63 and Alix.

HucMSC-Exo Labeling and Cellular Uptake

Exosomes were stained for visibility using the PKH67 green fluorescent dye according to the manufacturer's protocol from Solarbio (China). This involved mixing the HucMSC-Exo with PKH67 and Diluent C for 5 minutes, before stopping the reaction with the addition of 1% FBS. The fluorescent HucMSC-Exo were then introduced into an ultrafiltration tube to discard excess dye, using centrifugation at 4000g for 30 minutes. In vitro studies included co-culturing primary neutrophils with labeled exosomes and imaging following Hoechst 33,258 staining. In vivo studies involved injecting mice subdermally with the labeled exosomes and imaging using an IVIS Lumina Series III system. Post-injection at various time points, tissues were harvested, stained with DAPI, and observed under confocal microscopy.

Wound Healing Model and Treatment

Female 6~8 weeks old C56BL/6N mice, including diabetic and non-diabetic individuals, were prepared for skin wound experiments. All experimental procedures adhered to relevant international regulations outlined in the Guide for the Care and Use of Laboratory Animals. The study was approved by the Institutional Animal Ethics Committee for animal experiments. An electric clipper and 70% ethanol prepared the site for a sterile 8 mm biopsy punch incision. Wound healing progress was photo-documented every two days. HucMSC-Exo treatments (100 μg in 100 μL) occurred bi-daily. Wound diameters were measured in Photoshop to calculate closure rates.

Neutrophil Depletion in Live Mice

For neutrophil depletion studies, mice received an intraperitoneal injection of an anti-Ly6G antibody (200 μg per mouse) one day before starting HucMSC-Exo treatment. At the study endpoint, mice were sacrificed, and the efficacy of neutrophil depletion was assessed using flow cytometry. This analysis provided quantitative verification of the reduction in neutrophil populations, confirming the successful implementation of the neutrophil-depleting strategy.

In vivo Adoptive Transfer of CD11b+Ly6G+ N2-Neutrophils

For the adoptive transfer of N2-neutrophils, neutrophils were isolated from the bone marrow of Donor mice using the MACS-based neutrophil isolation kit (Miltenyi Biotec) following the manufacturer's recommendation. The isolated neutrophils were then subjected to HucMSC-Exo-driven polarization. Recipient mice were subcutaneously injected with a single injection of N2 neutrophils (10×10^6) resuspended in ice-cold HBSS in a volume of 100 μL at the indicated time

point. This adoptive transfer aimed to introduce polarized N2-neutrophils into the recipient mice for further investigation and analysis.

Generation of Conditioned Medium

Conditioned medium (CM) was created by incubating 1–2×10^6 primary neutrophils with or without 100 μg HucMSC-Exo in 10% FBS-supplemented RPMI media for 12 hours. After a PBS wash, the cells were incubated for another 12 hours in serum-free conditions. The harvested CM was centrifuged at 300×g for 10 minutes to clear out cells and debris, then frozen at −80°C for future experiments.

Cell Proliferation

Cell proliferation of SVEC4-10 targeted by the CCK-8 assay in 96-well plates. In brief, cells were treated with PBS, N0-CM, and HucMSC-Exo-polarized N2-CM for 24 h, 48 h, and 72 h, with optical density (OD) readings taken at 450 nm after a 2-hour treatment with a CCK-8 solution (Dojindo, Japan). EdU incorporation visualized with the BeyoClickTM EdU Kit (Beyotime, China) with Alexa Fluor 488 provided further cell proliferation insights.

Cell Migration and Invasion Assessments

The cell migration capacities were quantified using scratch assays. SVEC4-10 cells were plated in six-well plates and grown until they occupied 90% of the surface. A scratch was then made with the narrow end of a 10 μL pipette tip. The medium supplemented with different conditions similar to those in cell proliferation assays. Cell migration was documented at 0, 12, 24, and 48 hours post-scratch by photographing under a microscope. ImageJ software analysis provided cell migration figures and the scratch's gap measurements. The migration rate was computed with the formula: cell migration rate = [(original gap width - gap width at 12, 24, or 48 hours) / original gap width] × 100%. The cell invasion capacities were quantified using transwell assays, with migrated cells stained with crystal violet and observed under an optical microscope.

Tube Formation Assay

A 96-well plate was prepped with 50 μL of Matrigel, set at 37°C for 30 minutes. SVEC4-10 endothelial cells were then cultured at 20,000 cells per well in conditions akin to those used in the proliferation study. Post 6 hours incubation, tube structures were imaged via microscopy, with total branch points quantified using ImageJ software.

SiRNA Transfection

For silencing the specific gene, small interfering RNAs for BV8 (siBV8) and STAT6 (siSTAT6) were designed using the GenBank Accession Number: NM_001037539, NM_001178078, respectively. Provided by GenePharma, their sequences are listed in Table S1. After applying the transfection agent for 6 hours, cell media was refreshed. Post-transfection, knockdown efficiency in neutrophils was verified by qRT-PCR.

Immunofluorescence

Formalin-fixed, paraffin-embedded tissue sections were de-waxed, rehydrated, and underwent antigen retrieval. To block endogenous peroxidase activity, sections were treated with 3% H_2O_2 and further blocked with 3% BSA for 1 hour. Tissue sections were decorated with anti-mouse antibodies against CD31 (1:100, Abcam), Arg1 (Proteintech, 1:400), Ly6G (ThermoFisher, 1:1000), and p-STAT6 (1:100, Cell Signaling Technology) for 12 hours at 4 °C, secondary antibodies for an hour at room temperature, and DAPI to tag nuclei. An inverted fluorescence microscope captured the staining results, measured by ImageJ software.

Flow Cytometry

For flow cytometry analysis, cellular suspensions from skin samples (n=3) were washed once with PBS and permeabilized using eBioscience™ Foxp3/Transcription Factor Staining Buffer Set (catalog. 00-5523-00) following the manufacturer's instructions. Conjugated antibodies were added and incubated for 1 hour at room temperature. The antibodies

used included Alexa Fluor™ 700-CD11b (eBioscience, 56-0112-80, 1:100), FITC-Ly-6g (eBioscience, 11-5931-82, 1:400), PE-iNOS (eBioscience, 12-5920-80, 1:300), and APC-Arginase (eBioscience, 17-3697-80, 1:100). A flow cytometer recorded cell fluorescence, with FlowJo software analysis and appropriate control antibodies ensuring data accuracy.

Western Blot Analysis

Protein concentrations in cell and tissue extracts were quantified using the bicinchoninic acid protein assay prior to separation by SDS-PAGE. Proteins were then moved to PVDF membranes, blocked with 5% BSA, and incubated with primary antibodies at 4 °C, followed by incubated with HRP-conjugated secondary antibodies for 1 hour at room temperature. Detection was via the LAS-3000 Luminescent Image Analyzer.

Reverse Transcription-Quantitative PCR

RNA extraction was carried out using the RNA Easy Fast Tissue/Cell Kit (TIANGEN, DP451). The concentration of cell-free total RNAs was determined using NanoDrop 2000. Subsequently, cDNA was synthesized with the ReverTra Ace qPCR RT Master Mix with gDNA remover (FSQ-301; Toyobo) kit. For quantitative reverse transcription PCR (qRT-PCR), the SYBR Green Kit (Vazyme, Nanjing, China) was employed. GAPDH served as the internal control for normalization. The specific primer sequences can be found in Table S2.

JC1 Staining

Bone marrow-derived neutrophils were treated with PBS, HucMSC-Exo, or HucMSC-Exo plus AS1517499 for 12 hours. Neutrophils were stained with JC1 (Solarbio, China) for 20 minutes at 37°C. Fluorescent signals were visualized and captured using a fluorescent inverted microscope.

ATP Quantification

Neutrophils were treated with PBS, HucMSC-Exo, or HucMSC-Exo plus AS1517499 for 12 hours. ATP was assessed using the Cell Counting Kit-Luminescence Assay Kit (Dojindo, Japan).

Fatty Acid Uptake

Neutroplils were treated with PBS, HucMSC-Exo, or HucMSC-Exo plus AS1517499 for 12 hours. Fatty acid uptake in neutrophils were assessed using the Fatty Acid Uptake Assay Kit (Dojindo, Japan). Fluorescent signals were visualized and captured using a fluorescent inverted microscope.

Statistical Analysis

All statistical analyses in this study were conducted using GraphPad Prism 8 InStat Software (San Diego, CA, USA). The data were presented as the mean ± SEM from at least three separate trials. Group comparisons involved the Student's *t*-test or ANOVA, with a p-value below 0.05 marking statistical significance. Statistical tiers were annotated as *p < 0.05, **p < 0.01, ***p < 0.001, ****p < 0.0001.

Results

Characterization of HucMSC-Exo

After purification, we conducted NTA analysis, TEM, and Western blotting analysis to characterize the size, morphology, and surface marker expression of purified nanoparticles derived from huc-MSCs. NTA measurement revealed a medium diameter of 102.6 nm (Figure 1A), consistent with reported HucMSC-Exo size distributions. TEM displayed a round vesicle-shaped morphology (Figure 1B), typical of HucMSC-Exo. Furthermore, exosomal markers CD63 and Alix were identified through Western blotting analysis (Figure 1C), confirming the identity of these nanoparticles as HucMSC-Exo.

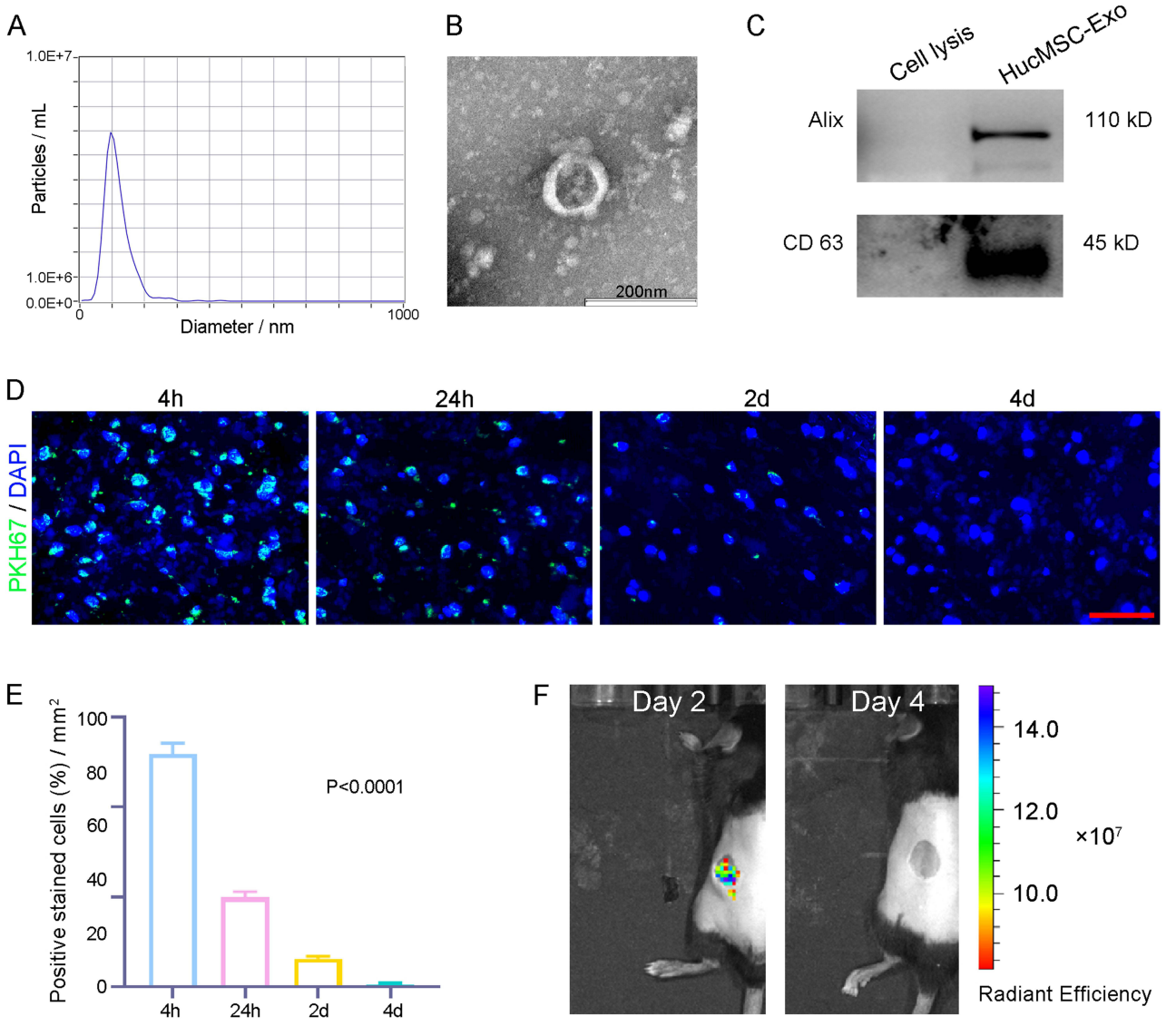

Figure 1 Characterization and retention of HucMSC-Exo in cutaneous wound tissues. (**A**) Measurement of the particle size distribution of HucMSC-Exo by nanoparticle tracking analysis. (**B**) Morphological features of HucMSC-Exo observed by transmission electron microscope. Scale bar = 200 nm. (**C**) Surface markers of HucMSC-Exo detected by Western blotting. (**D**) Typical images of skin tissue uptaking HucMSC-Exo at different time point. Scale bars, 50 μm. (**E**) Quantification of the amount of skin cells that uptake PKH67-labeled hHcMSC-Exo at indicated times in (**D**). n = 3 per group. All P < 0.0001 compared with the 4 h group. (**F**) Representative in vivo imaging picture of retention of PKH67 labeled HucMSC-Exo at day 2 and day 4 on wound.

Retention of HucMSC-Exo in Skin Tissues

We investigated the retention of HucMSC-Exo within dermal tissues using fluorescence microscopy post-injection. Four hours after administration, a considerable accumulation of PKH67-stained HucMSC-Exo was evident around the peri-nuclear zones of dermal cells. However, the signal intensity decreased by 24 hours; by 2 days after injection, HucMSC-Exo were significantly less dense in skin tissues. By day 4, no fluorescent signal was detected (Figure 1D). Quantitative analysis confirmed a time-dependent decline in uptake of the labeled exosomes around the wound sites (Figure 1E). These findings suggest that transplanted HucMSC-Exo led to a gradual reduction in stimuli for resident skin cells over time.

Before exploring wound healing effects, real-time fluorescence imaging analysis was employed to investigate the in vivo biodistribution of HucMSC-Exo (Figure 1F). The PKH67-labeled HucMSC-Exo fluorescence signal persisted well in subcutaneous tissue for more than 2 days, gradually reducing. By day 4 post-subcutaneous injection, the

fluorescence dropped to under 10%. This observation substantiates that subcutaneously injected HucMSC-Exo have sufficient time for potentially inducing local cellular phenotype reprogramming (Figure 1F).

In situ Wound Healing Effect of Hucmsc-Exo Relied on Neutrophil Infiltration

During the wound healing process, activated myeloid cells, including neutrophils and macrophages, infiltrate the wound site. Our prior recognition of the participation of myeloid cells, specifically macrophages and neutrophils, in the wound healing process led us to investigate their role in HucMSC-Exo-guided wound healing.[16] We deployed two strategies to selectively deplete either circulating monocytes (via anti-F4/80 treatment) or neutrophils (via anti-Ly6G) in recipient mice (Figure 2A). Intraperitoneal injection of the anti-Ly6G antibody resulted in the effective depletion of neutrophils without affecting circulating monocytes. Conversely, anti-F4/80 treatment selectively depleted circulating monocytes while sparing neutrophils (Figure 2B). Depletion of circulating monocytes through anti-F4/80 treatment did not significantly impact wound healing and vascularization; HucMSC-Exo injected into F4/80-treated mice exhibited a microvascular density comparable to the control group (Figure 2C-E). In contrast, the depletion of neutrophils via anti-Ly6G had a detrimental effect on wound healing and vascularization. Mice treated with anti-Ly6G and injected with HucMSC-Exo displayed reduced vascularization compared to the control group (Figure 2C-F). These results stress the critical reliance of HucMSC-Exo's wound repair function on the presence of infiltrating neutrophils.

Adoptive Transfer Bone Marrow (BM)-Derived Neutrophils Rescued Vascularization

To further validate the pivotal function of neutrophils, we implemented an adoptive transfer strategy using neutrophils-depleted mice. In this approach, HucMSC-Exo were implanted into mice depleted of neutrophils, with or without the transfer of neutrophils from non-depleted donor mice (Figure 2G). To obtain neutrophils, we utilized a magnetic associated cell sorting protocol to purify a predominantly mCD11b+/mLy6G+ neutrophil population, ensuring a 98% purity (Figure S1). HucMSC-Exo implanted into neutrophils-depleted mice exhibited delayed vascularization. However, the adoptive transfer of BM-derived neutrophils partially restored vascularization, resulting in a mature network of blood vessels (Figure 2H and I). An experiment utilizing blood-origin mLy6G+ cells also aided vascularization, albeit less effectively (Figure 2I). Notably, the transfer of F4/80+ cells, identifying monocytes/macrophages, did not yield similar restorative effects on the vasculature (Figure 2I), emphasizing the distinctive and indispensable contributions of neutrophils to this phase of healing. Adding complexity to this scenario, confocal microscopy demonstrated that transferred neutrophils were predominantly localized at branch points and integrated into the vessel network (Figure 2J), indicating a potential crosstalk between these cells. Intriguingly, neutrophils localized chiefly around nascent vessels rather than matured ones, likely because the fact that mature vessels had finalized their remodeling phase. In summary, these comprehensive results authenticate the indispensable role of host $mLy6G^{+}$ neutrophils in promoting vascularization during skin wound healing.

HucMSC-Exo Induces Phenotypic Switching of Neutrophils to the N2 Subtype

A range of studies has brought neutrophils' remarkable plasticity to the fore, detailing how LPS+IFN-gamma can induce a pro-inflammatory N1 state, while IL-4 can orient neutrophils towards an anti-inflammatory N2 phenotype, analogous to the M1 and M2 classifications in macrophages.[18–20] Building on our prior investigation,[16] which demonstrated that HucMSC-Exo increased the abundance of M2 macrophages, we aimed to investigate whether HucMSC-Exo could induce a similar phenotype switch in neutrophils. To achieve this, myeloid neutrophil cells were isolated using MACS cell sorting kits, and BM-derived neutrophils were incubated with HucMSC-Exo (Figure 3A). Following a 12-hour incubation period, the expression of N1 and N2-related markers was assessed using qRT-PCR. The results demonstrated that treatment with HucMSC-Exo induced a significant shift of neutrophils towards the N2 phenotype, with a surge in N2 marker expression, including Arg1, CD163, and CD206 (Figure 3B). To further validate this phenomenon in vivo, we examined whether HucMSC-Exo could drive the phenotype switch of wound-resident neutrophils towards an anti-inflammatory N2 phenotype (Figure 3C). After direct application of HucMSC-Exo to an excisional skin wound in mice through subcutaneous injection around the wound, flow cytometry was employed to measure the phenotype switching of neutrophils. At 24 hours post-insult, approximately one-third of the neutrophils in the wound area were found to be

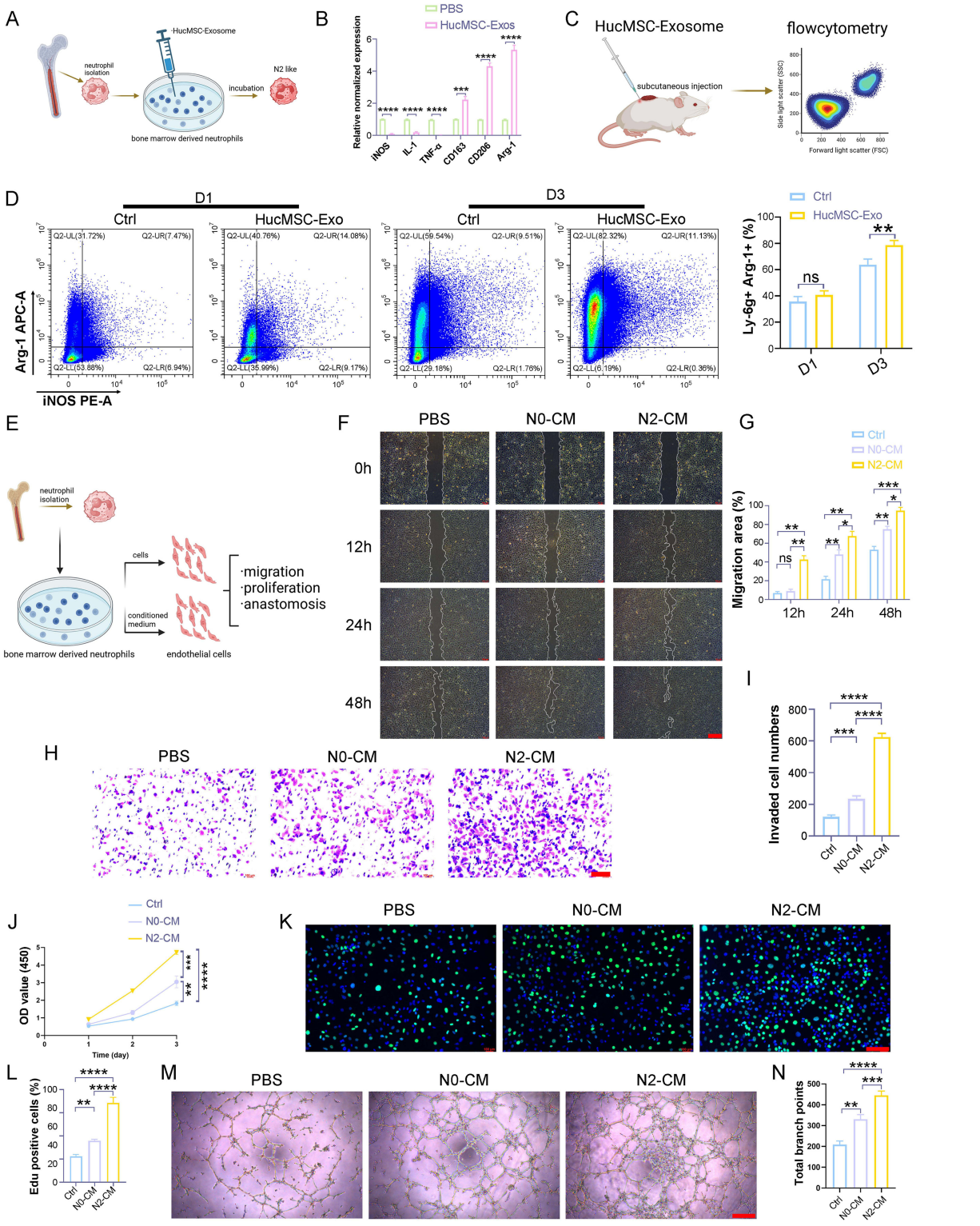

Figure 2 HucMSC-Exo-polarized N2 neutrophils showed enhanced proangiogenic ability. (**A**) Schematic diagram of the experimental procedure showing bone marrow-derived neutrophils incubated with HucMSC-Exo. (**B**) qPCR detects the transcriptional levels of N1 markers (iNOS, IL-1, TNF-α), and N2 markers (Arg1, CD163, CD206) in HucMSC-Exo treated neutrophils. (**C**) Schematic diagram showing in vivo phenotypic switching of neutrophils that triggered by HucMSC-Exo. (**D**) Flow cytometry and quantitative analysis of Arg1-positive cells in skin wound lesions treated with PBS or HucMSC-Exo at day 1 and day 3. (**E**) Schematic diagram of the experimental procedure of endothelial cell co-cultured with HucMSC-Exo-polarized N2 neutrophils. (**F**) Representative images of the scratch healing assay. (**G**) Quantification of repair area after incubating 12, 24, and 48 h. Scale bars, 300 μm. (**H**) Representative images of transwell invasion assay. Scale bars, 300 μm. (**I**) Quantification of migrated cell number in transwell assay. CCK8 assays (**J**) and fluorescence images (**K**) showing the proliferation capacity of endothelial cell treated with condition medium derived from different phenotype of neutrophils (green: EdU staining; blue: DAPI staining). Scale bars, 300 μm. (**L**) Quantification of portion of EdU positive cells (%). (**M**) Tube formation of endothelial cell treated with condition medium derived from different phenotype of neutrophils. Scale bars, 300 μm. (**N**) Quantification of total branch points representing tube formation ability. [*p < 0.05, **p < 0.01, ***p < 0.001, ****p < 0.0001; data were expressed as mean ± SD and analyzed by unpaired two-tailed *t*-test].

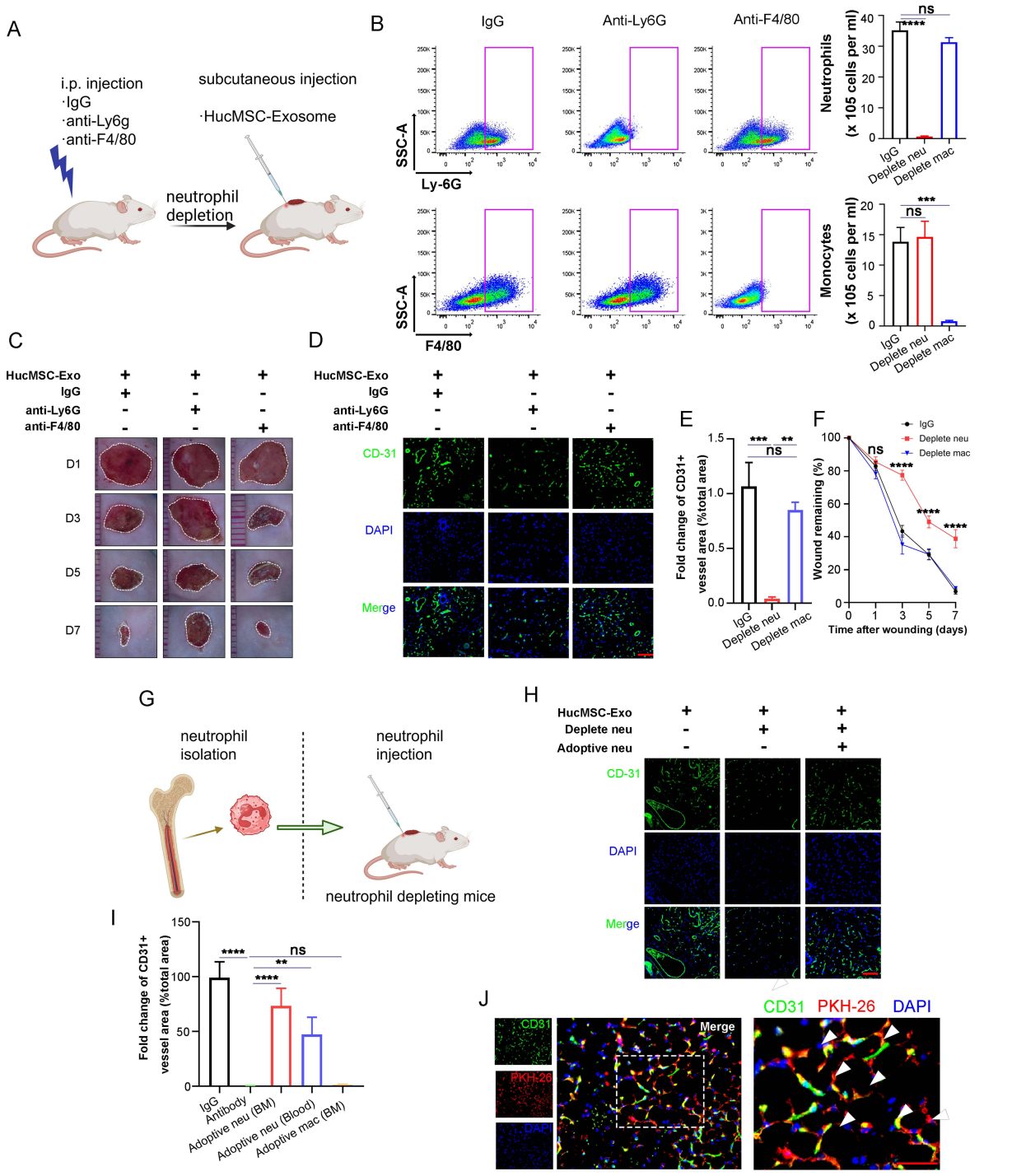

Figure 3 The healing effect of HucMSC-Exo on wound relies on infiltrated neutrophil. (**A**) Schematic diagram of myeloid depletion strategies. (**B**) Flow cytometry analysis of blood samples after different depletion treatments. The gross view of wounds (**C**) and immunofluorescence stained CD31 (**D**) of HucMSC-Exo, HucMSC-Exo plus neutrophil depletion, and HucMSC-Exo plus macrophagy depletion groups at day 1, 3, 5 and 7. Scale bars, 100 μm. Quantification of the wound closure (**E**) and fold change of CD31+ vessel area (% total area) (**F**). n = 3 per group. (**G**) Schematic diagram for adoptive transfer (ADT) of host neutrophils. (**H**) In vivo distribution of CD31 labeled neovessels in wound treated with HucMSC-Exo, HucMSC-Exo plus neutrophil depletion, and HucMSC-Exo plus neutrophil depletion plus adoptively transferred neutrophils. Scale bars, 100 μm. (**I**) Quantification of fold change of CD31+ vessel area (% total area). (**J**) Co-localization of fluorescent-labelled endothelial cells (green) and neutrophil (red). Scale bars, 50 μm. Arrows mark the merging of neutrophils into the network structure. [**p < 0.01, ***p < 0.001, ****p < 0.0001; data were expressed as mean ± SD and analyzed by unpaired two-tailed *t*-test].

Arg1^{+}, with this percentage not significantly affected by HucMSC-Exo. However, by day 3, a notable shift occurred, indicating that HucMSC-Exo significantly skewed neutrophils towards a Ly-6g^{+}Arg1^{+} neutrophil population, characteristic of the N2 subtype, achieving an exceptionally high conversion efficiency of approximately 85% (Figure 3D).

Effects of HucMSC-Exo-Polarized Neutrophils on Angiogenesis in vitro

While it is recognized that myeloid cells play an essential role in the processes of neovascularization and angiogenesis,[21–23] there has been a more pronounced emphasis on how monocytes and macrophages influence tumor angiogenesis.[24–26] However, emerging evidence points to a noteworthy contribution of neutrophils to angiogenesis.[27] To pinpoint the specific effect of HucMSC-Exo-polarized N2 neutrophils on vascular function, a series of assays evaluating endothelial cell proliferation, migration, invasion, and vascular anastomosis were conducted using conditioned medium and co-culture in vitro (Figure 3E). The initial focus was on evaluating the impact of conditioned media derived from HucMSC-Exo-polarized N2 neutrophils (N2-CM) on scratch repair (Figure 3F). Naïve neutrophil-derived conditioned media (N0-CM) served as a control. At 12 and 24 hours, the N2-CM group exhibited a significantly superior repair capability compared to the N0-CM group. Even at 48 hours, a substantial unrepaired area persisted in the N0-CM group (Figure 3F and G). Additional examination under co-culture conditions demonstrated that the co-cultured N2 neutrophils alongside endothelial cells notably boosted the repair rate in contrast to N0 neutrophils (Figure S2). Transwell assays corroborated these findings, with the N2-CM treated group showing the highest levels of invaded endothelial cells among all tested groups (Figure 3H and I). Further focus on the proliferation capacity of endothelial cells revealed that the N2-CM group had a slight proliferation advantage over the control or N0-CM within the initial 24 hours, with this capacity increasing at 48 and 72 hours, as indicated by CCK-8 assay results (Figure 3J). This cell proliferation trend was further supported by EdU assay data. The prevalence of green-fluorescing endothelial cells—which designates their active proliferation—revealed that HucMSC-Exo-polarized N2 neutrophils had the highest pro-proliferation ability (Figure 3K and L), aligning with the observations from the CCK-8 results.

Acknowledging that sprouting and subsequent vascular anastomosis are vital for effective vascular regeneration, a tube formation assay was conducted, which crucially illustrated the influence of phenotypically distinct neutrophils on this process. The results indicated that endothelial cells stimulated with N2-CM showcased a stark enhancement in their capacity to establish capillary structures in contrast to those interacting with N0-CM (Figure 3M and N).

Secreted BV8 by HucMSC-Exo-Activated N2 Neutrophil Promotes the Angiogenesis of Endothelial Cells

Investigating further into the molecular mechanisms, a gene expression profile analysis on mouse primary neutrophils – with and without HucMSC-Exo treatment – was performed focused on angiogenesis-related genes. This analysis brought to light that BV8 (prokineticin-2), a secretory glycoprotein found within neutrophil granules and known to be highly mitogenic for endothelial cells, was dramatically upregulated in HucMSC-Exo-activated N2 neutrophils as opposed to the control cells (Figure 4A). BV8 is recognized as a pivotal angiogenic factor, especially within the realm of neutrophil-dependent tumor angiogenesis.[28] Confirmation of these findings came via ELISA analysis, which showed that both mouse primary neutrophils and human HL-60 neutrophil cells released more BV8 following exposure to HucMSC-Exo than untreated neutrophils (Figure 4B). Moreover, the upregulation of BV8 in wounds treated with HucMSC-Exo, and the attenuation of this trend upon neutrophil depletion, was also observed (Figure 4C). Prior study showed $CD11b^{+}Ly\text{-}6G^{+}$ neutrophils mediate tumor angiogenesis by producing various proangiogenic factors, most notably Bv8. To delineate the exact role of BV8 in inducing angiogenesis, endothelial cells were treated with mouse recombinant BV8 (mrBV8). At a low concentration (1 μM), mrBV8 spurred angiogenesis in endothelial cells, accompanied with strong HIF-1α expression (Figure 4D and E), while intriguingly, VEGFα expression in the BV8-treated group did not show any significant alteration, suggesting BV8's critical involvement in VEGF-independent angiogenesis (Figure 4E).

Furthermore, to directly assess the influence of BV8 secreted by N2-neutrophils on angiogenesis, siRNA technology was utilized to knockdown BV8 in neutrophils. In vitro testing revealed a significant decrease in angiogenesis upon treatment with CM derived from HucMSC-Exo-treated BV8-knockdown N2 neutrophils, as opposed to the control (wild-type) (Figure 4F). Further tested in vivo, when BV8 knockdown neutrophils were adoptively transferred into neutrophil-depleted mice, the loss of BV8 significantly correlated with decreased angiogenesis compared to those with normal BV8 expression (Figure 4G). These cumulative results indicate that HucMSC-Exo-activated N2 neutrophils partially enhance angiogenesis by prompting the release of BV8.

A

Differently expressed genes in HucMSC-Exo treated mouse primary neutrophils			
Gene	Fold Change	P.Value	adj.P.Val
BV8	7.4	6.15E-05	0.000042
VEGFα	5.3	0.000216	0.001649
MMP9	4.6	0.000360	0.000334
FGF1	3.7	0.002481	0.087492
VEGFB	3.3	0.005294	0.000682
PDGFα	3.1	0.000264	0.000452
EGLN3	2.8	0.000245	0.001104
ANG	2.7	0.005329	0.000485
TIMP3	2.7	0.001328	0.000257
CXCL6	2.7	0.004764	0.000391
FLT1	2.6	0.009247	0.003895
ANPEP	2.6	0.010485	0.000529
CXCL10	2.5	0.007462	0.000385
ANGPTL4	2.5	0.015274	0.008258

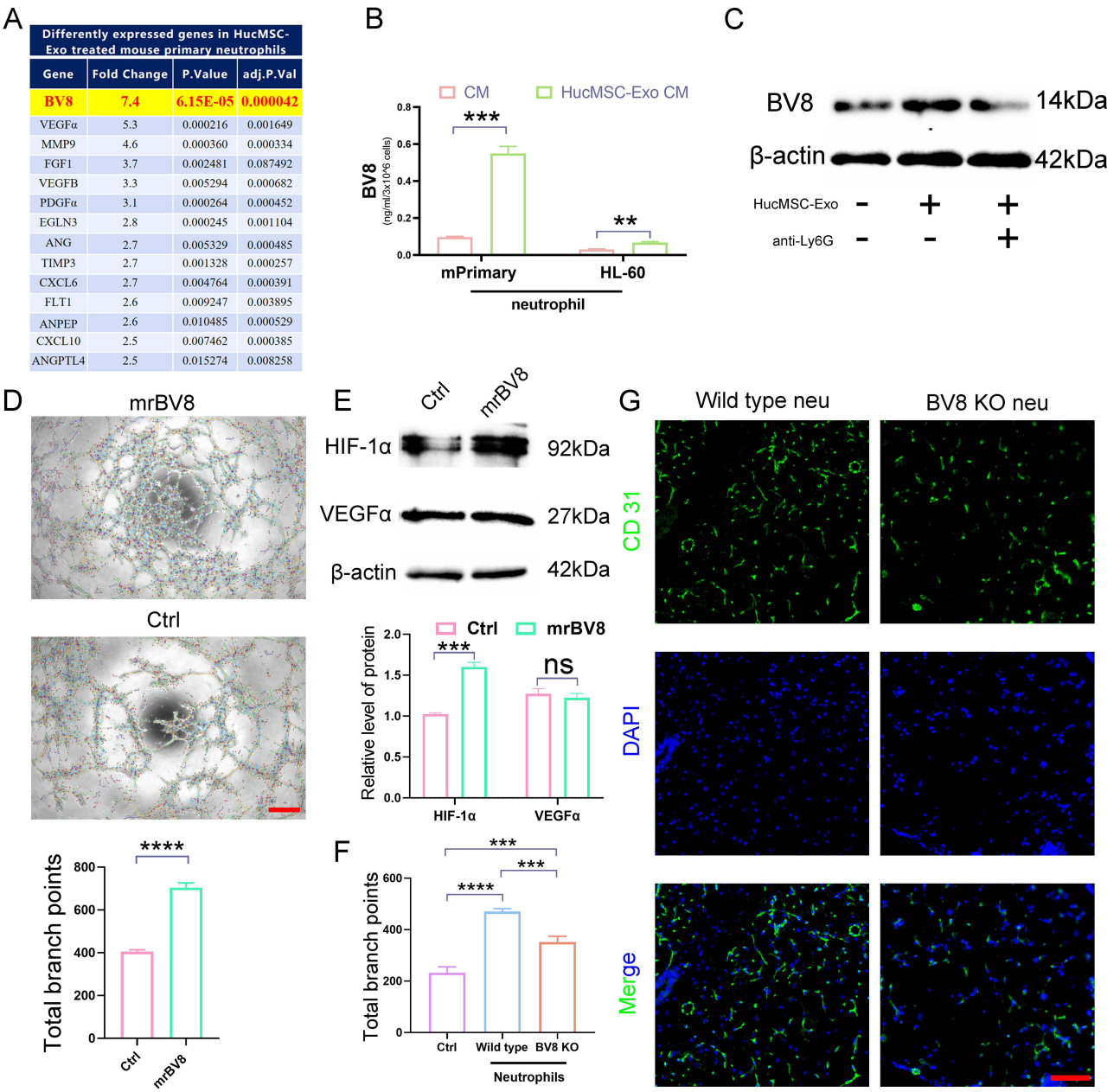

Figure 4 BV8 Secreted by HucMSC-Exo-polarized N2 neutrophil promotes angiogenesis. (**A**) Mouse primary neutrophils were subjected to treatment with or without HucMSC-Exo for 12 h, followed by examining the expression of a series of secretory factors that are involved in angiogenesis. (**B**) BV8 protein levels in condition medium derived from HucMSC-Exo treated or untreated neutrophils (mouse primary and human HL-60 cells) were quantified by ELISA. (**C**) Representative Western blotting images of BV8 in skin wound after treated with HucMSC-Exo or HucMSC-Exo plus neutrophil depletion. (**D**) Tube formation of endothelial cells treated with or without 1μm mouse recombinant BV8. Scale bars, 300 μm. (**E**) Representative Western blotting images of HIF-1α and VEGFα from endothelial cells treated with or without 1μm mouse recombinant BV8. (**F**) Tube formation of endothelial cells treated with condition medium derived from wild type or BV8 knockdown neutrophils. (**G**) In vivo distribution of CD31 labeled neovessels in wounds treated with adoptively transferred wild-type or BV8 knockdown neutrophils. Scale bars, 100 μm. [**p < 0.01, ***p < 0.001, ****p < 0.0001; data were expressed as mean ± SD and analyzed by unpaired two-tailed *t*-test].

HucMSC-Exo Spurs Mitochondrial Metabolic Reprogramming in Neutrophils via the Jak2/STAT6 Pathway

In the course of M2-like polarization, STAT6 signaling pathways, in collaboration with peroxisome proliferator-activator receptor gamma (PPARγ), propel macrophage metabolism towards the mitochondrial beta-oxidation of fatty acids and oxidative phosphorylation for energy production.[29] In an attempt to discern if HucMSC-Exo elicited comparable reactions in neutrophils, protein expression levels of p-Jak1/2, STAT1/3/6, and p-STAT1/3/6 were analyzed through

Western blotting after HucMSC-Exo or PBS treatments. The results revealed that HucMSC-Exo significantly increased the phosphorylation of Jak2 and STAT6 while markedly decreasing the expression of p-STAT1 (Figure 5A).

Recognizing STAT6's importance in lipid metabolism—enhancing fatty acid oxidation (FAO) and energy generation in M2 macrophages—a selective STAT6 inhibitor, AS1517499, was employed to assess its effect.[30] This inhibitor, in a dose-responsive manner, suppressed STAT6 function in HucMSC-Exo-stimulated neutrophils and counteracted the surge in mRNA levels of PPARγ and FAO genes (*Cpt1b, Acadm*, and *Acadl*) (Figure 5B-D). Post HucMSC-Exo treatment, fatty acid uptake in neutrophils rose, yet this was mitigated by inhibiting STAT6 expression (Figure 5E).

These findings resonate with previous research indicating that nuclear receptors, through metabolic shifts, contribute to M2-like polarization, marking PPARγ as a regulator of FAO for ATP production to maintain cellular functions.[31] The reduced FAO in AS1517499-treated neutrophils correlated with significantly diminished ATP levels, highlighting a bioenergetic redirection akin to the metabolic profile changes observed in M1 and M2 macrophages (Figure 5F). It has been established that M2 macrophages rely on oxidative metabolism for prolonged energy generation to maintain wound healing and tissue repair functions.[32] Our metabolomic analysis corroborated this energetic shift, identifying significant modifications in OXPHOS and glycolysis initiated by HucMSC-Exo (Figure 5G). Interestingly, AS1517499 dampened oxidative metabolism in HucMSC-Exo-treated neutrophils, suggesting that HucMSC-Exo induced a bioenergetic recalibration in neutrophils that was attenuated when STAT6 signaling was impeded (Figure 5G). Moreover, mitochondria in HucMSC-Exo-treated neutrophils showed heightened membrane potential, distinguished by an increased number of red-fluorescent aggregates from JC-1 staining, unlike the AS1517499-treated cells that exhibited a higher count of mitochondria with low membrane potential (Figure 5H).

HucMSC-Exo Sknewed Neutrophil Toward a N2 Phenotype in a STAT6-Dependent Manner

The role of HucMSC-Exo in skewing neutrophils towards an N2 phenotype was further demonstrated to be STAT6-dependent, particularly in the transcriptional control of Arg1, a hallmark of the N2 state.[33] Examination revealed that HucMSC-Exo treatment substantially pushed neutrophils towards the N2 phenotype (Arg1+), while STAT6 inhibition decreased Arg1 activity in a dose-responsive manner (Figure 6A). Human neutrophils (HL-60 cells) treated with HucMSC-Exo in the presence of AS1517499 also displayed significant downregulation of N2-associated markers (Figure S3A). Further corroboration was achieved by treating HL-60 cells with HucMSC-Exo in the absence or presence of STAT6-specific siRNA, leading to a notable reduction in Arg1 expression (Figure S3B). Additionally, dose-dependent downregulation of BV8 was apparent in HucMSC-Exo-treated N2-neutrophils in the presence of AS1517499 (Figure S3C). The in vivo study showed a significant decreased in p-STAT6 expression in the mice wound site treated with AS1517499 (Figure 6B). Evaluation of the activation status of STAT6 in $CD11b^{+}Ly\text{-}6g^{+}$ neutrophils on the wound site revealed that HucMSC-Exo induced STAT6 phosphorylation, while AS1517499 mitigated STAT6 activity within $CD11b^{+}Ly\text{-}6g^{+}$ neutrophils in vivo (Figure 6C). Immunofluorescence analysis of relevant N2 neutrophil markers on the wound site demonstrated that HucMSC-Exo induced the polarization of N2-neutrophils (Arg1), which was dampened by AS1517499, indicating that STAT6 blockage in vivo attenuated this phenotypic switching process driven by HucMSC-Exo (Figure 6D). Furthermore, HucMSC-Exo treatment in the presence of AS1517499 significantly dampened wound neoangiogenesis and impeded the wound healing process, underscoring that HucMSC-Exo-facilitated wound healing hinged on STAT6 activation in N2-neutrophils (Figure 6E-H). These results suggests that the augmentation of wound healing response to HucMSC-Exo involves N2-neutrophils energized through STAT6 signaling.

Neutrophils Failed to Skew Toward N2 Phenotype in Diabetic Wounds

In comparison to normal healing processes, wounds in diabetics show slower closure rates, extended periods of inflammation, and suboptimal blood vessel formation.[34] Based on the aforementioned findings, we are interested in determining whether there are deficiencies in the transition process of neutrophils to the N2 phenotype during wound healing process in the context of diabetes. Initially, we conducted an examination to assess the extent of neutrophil infiltration in wound throughout the healing process. As shown in Figure 7A, on days one and three, the number of

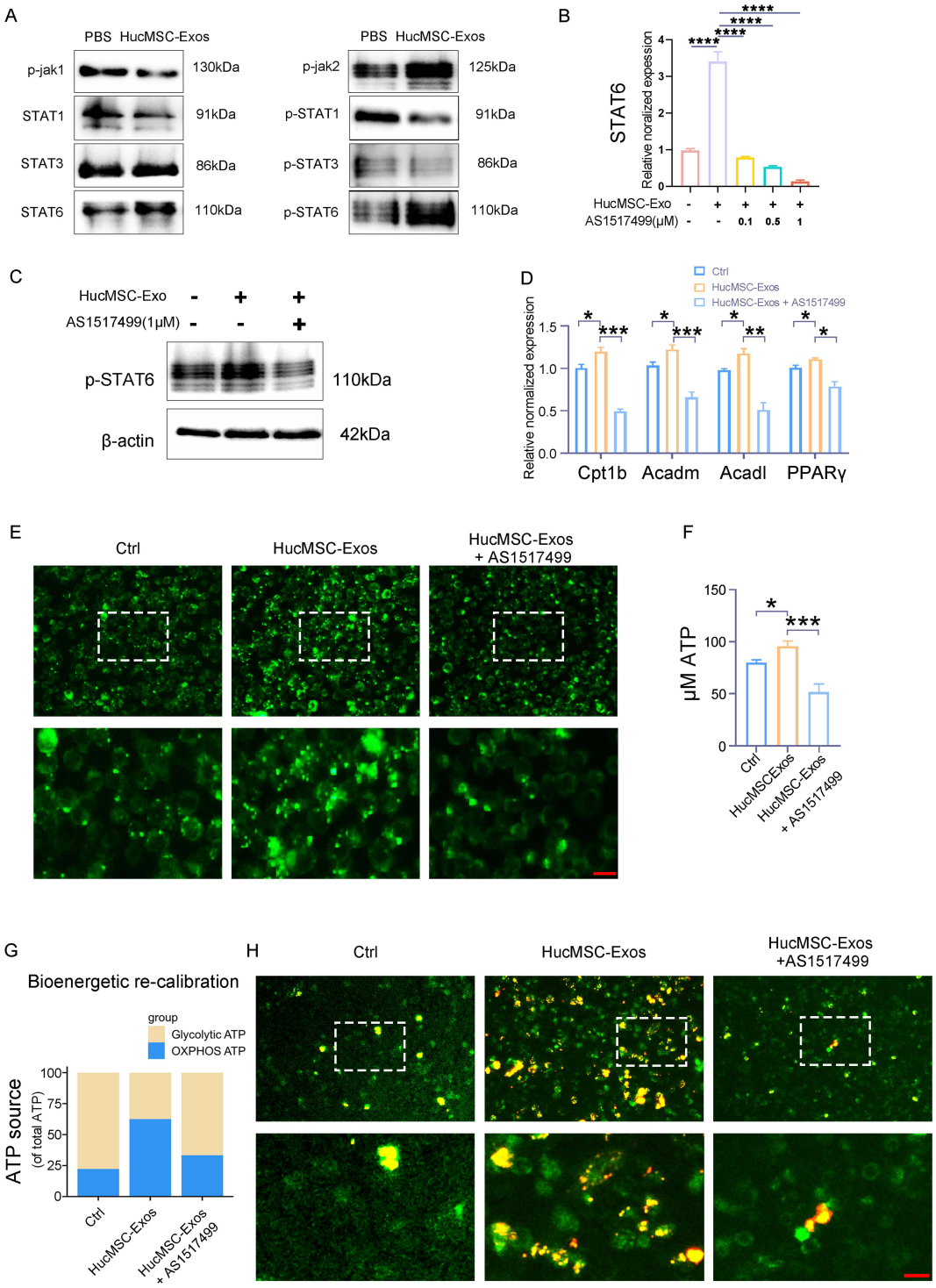

Figure 5 HucMSC-Exo induced mitochondrial Metabolic recalibration in neutrophils in a STAT6-dependent manner. (**A**) Mouse primary neutrophils were treated with HucMSC-Exo for 12 h, and examined for p-Jak1/2, STAT1/3/6 and p-STAT1/3/6 expression by Western blot. β-actin was used as controls (n = 3 individual experiment/group). (**B**) Mouse primary neutrophils were treated with HucMSC-Exo or AS1517499 at various concentrations and STAT6 expressions were examined by qRT-PCR. GAPDH was used as a normalization control (n=3). (**C**) Representative Western blotting images of p-STAT6 from mouse primary neutrophils treated with HucMSC-Exo or AS1517499 (1 μM). (**D**) Transcript levels of PPARγ and FAO genes (*Cpt1b, Acadm*, and *Acadl*) in mouse primary neutrophils treated with HucMSC-Exo or HucMSC-Exo plus AS1517499 (1 μM). (**E**) Fatty acid uptake was analyzed in mouse primary neutrophils treated with HucMSC-Exo or HucMSC-Exo plus AS1517499 (1 μM). Scale bars, 50 μm. (**F**) Cellular ATP content in mouse primary neutrophils. (**G**) ATP content of OXPHOS and glycolysis in mouse primary neutrophils. (**H**) Representative images of JC-1 staining in mouse primary neutrophils. The cationic dye JC-1 forms red fluorescent aggregates at high mitochondrial potentials and maintains green fluorescent monomers at low mitochondrial potentials. Scale bars, 50 μm. [*p < 0.05, **p < 0.01, ***p < 0.001, ****p < 0.0001; data were expressed as mean ± SD and analyzed by unpaired two-tailed *t*-test].

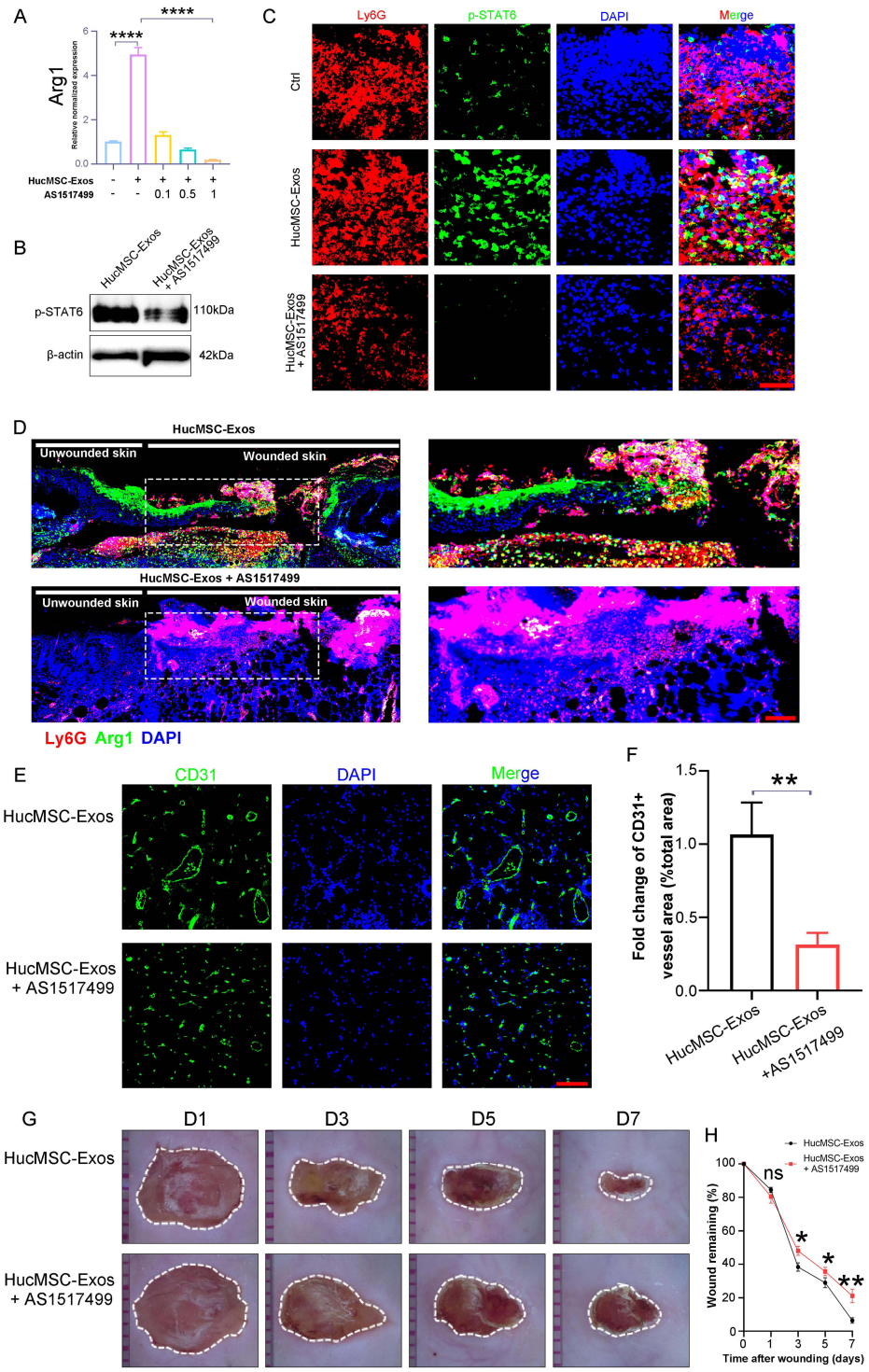

Figure 6 HucMSC-Exo induced STAT6 activation and thereby skewed neutrophil to an N2 phenotype. (**A**) Mouse primary neutrophils were treated with HucMSC-Exo or AS1517499 at various concentrations and Arg1 expressions were examined by qRT-PCR. GAPDH was used as a normalization control (n=3). (**B**) Representative Western blotting images of p-STAT6 from mouse wound lesson treated with PBS or HucMSC-Exo. (**C**) Representative immunofluorescence images of Ly6G+pSTAT6+ neutrophils in wound sections of HucMSC-Exo or HucMSC-Exo plus AS1517499s treated mice. Scale bars, 50 μm. (**D**) Representative immunofluorescence images of N2 (Arg1+) neutrophils in wound sections treated with HucMSC-Exo or HucMSC-Exo plus AS1517499s. (**E**) In vivo distribution of CD31 labeled neovessels in wounds treated with HucMSC-Exo or HucMSC-Exo plus AS1517499s. Scale bars, 100 μm. (**F**) Quantification of fold change of CD31+ vessel area (% total area). (**G**) The gross view of wounds from mouse treated with HucMSC-Exo or HucMSC-Exo plus AS1517499s at day 1, 3, 5 and 7. (**H**) Quantification of the wound closure. [*p < 0.05, **p < 0.01, ****p < 0.0001; data were expressed as mean ± SD and analyzed by unpaired two-tailed *t*-test].

infiltrating neutrophils in the diabetic wounds was comparable to that in normal wounds. However, by day five and day seven, the quantity of neutrophils in normal wounds began to decrease, while their numbers remained high in the diabetic wounds. We further verified the proportion of N2 subtype within the total neutrophil population. We discovered that, within the first seven days of wound healing, the proportion of N2 subtype neutrophils among the total neutrophil population in normal wounds progressively increased, reaching as high as 82.36% by day seven. In contrast, their proportion in diabetic wounds consistently remained below 10% (Figure 7B). Mechanically, we observed that molecule p-STAT6 within neutrophils is deactivated within the microenvironment of diabetic wounds (Figure 7C). Further investigations were conducted into the tissue-specific chemokine and cytokine profile influencing neutrophil recruitment and polarization. It was discerned that within diabetic wound sites, there were significant elevations in the levels of CCL2, CCL3, and CCL5, which are pivotal in mediating neutrophil recruitment (Figure 7D). Concurrently, there were noticeable decreases in the concentration of IL-4 and IL-13, cytokines crucial for the polarization towards an N2 neutrophil phenotype, whereas the levels of IFN-gamma, a cytokine essential for N1 neutrophil programming, were increased (Figure 7E). These findings elucidate the altered chemokine and cytokine milieu that may contribute to the dysregulated inflammatory response observed in diabetic wound healing. Meanwhile, the diminution of the N2 subtype within diabetic wounds was concomitant with impediments to angiogenesis (Figure 7F). Collectively, these observations highlighted a potential correlation between the reduced presence of N2 neutrophils and the compromised vascularization intrinsic to the pathophysiology of diabetic wound healing.

HucMSC-Exo Promotes Diabetic Wound Healing by Driving Neutrophil Polarization Toward Angiogenic N2 Phenotype

We further explored whether HucMSC-Exo could expedite the healing and revascularization process in diabetic wounds by encouraging neutrophil polarization toward N2 phenotype. In the context of diabetic wounds, the N2 subtype of neutrophils constituted less than 10%, but with the application of HucMSC-Exo, their proportion significantly increased to 80.37% (Figure 8A and B). Mechanistically, dormant p-STAT6 in neutrophils was reactivated under the influence of HucMSC-Exo (Figure 8C). With the rise in N2 subtype neutrophils, enhanced wound healing and increased vascularization were observed (Figure 8D-G). While previous researches had highlighted HucMSC-Exo's direct promotive effects on vascular endothelial cells and re-epithelialization,[35] our findings indicated an additional indirect healing facilitation through the modulation of neutrophil polarization to the N2 subtype. To ascertain the importance of HucMSC-Exo acting via neutrophils, we utilized AS1517499 to impede their polarization towards the N2 subtype. Subsequent to the use of AS1517499, inactivation of p-STAT6 was observed in neutrophils, abolishing the N2 polarization induced by HucMSC-Exo (Figure 8A-C). Notably, when N2 polarization was inhibited, the prohealing effects induced by HucMSC-Exo was diminished, accompanied by a reduction in neovascularization (Figure 8D-G). In summary, the gathered evidences underscore the significant role of HucMSC-Exo in not only directly promoting wound healing and revascularization, but also indirectly by modulating neutrophil polarization towards the N2 phenotype, highlighting the multifaceted actions of HucMSC-Exo in potential therapeutic strategies addressing diabetic wound management.

Discussion

Our study sheds light on the intriguing role of HucMSC-Exo in the polarization of neutrophils toward an M2-like, or N2 phenotype, an orientation that is coupled with enhanced angiogenesis and expedited healing of full-thickness skin wounds. While lymphocytes and macrophages have demonstrated the ability to switch phenotypes,[12] this study provides hitherto undocumented evidence of HucMSC-Exo-induced neutrophil reprogramming at the wound site, coinciding with improved healing outcomes.

To date, various research groups have highlighted the pro-healing properties of HucMSC-Exo in wounds, primarily attributed to their anti-inflammatory and antioxidant mechanisms.[1,3,5] In our investigation, we aimed to explore how HucMSC-Exo impacts the peripheral inflammatory response, specifically focusing on the orchestration of infiltrated neutrophils toward a pro-healing status. Contradictory findings from studies depleting neutrophils in animal models prompted us to delve into the role of neutrophils in our wound model. Interestingly, depleting circulating neutrophils

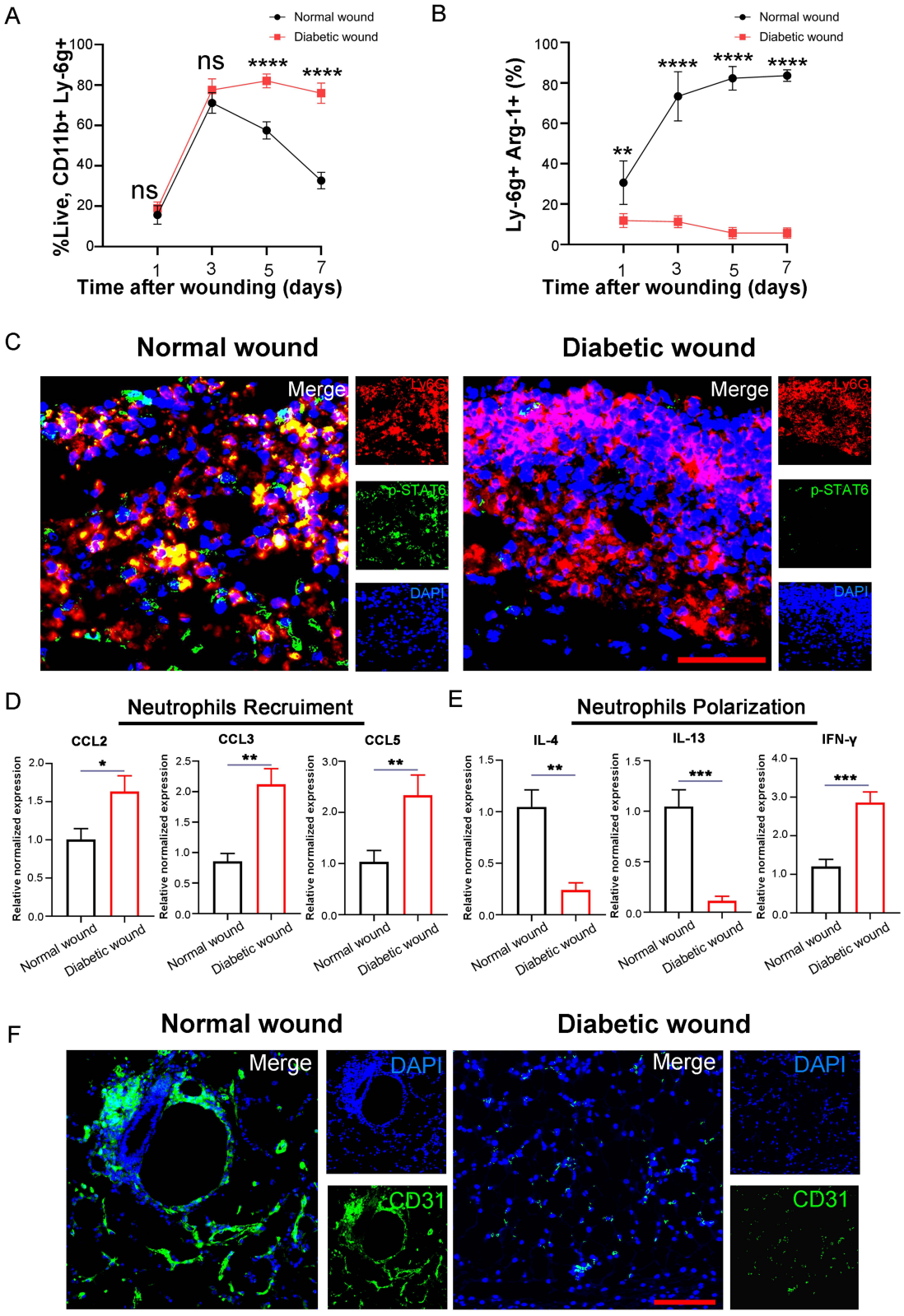

Figure 7 Neutrophils in diabetic wounds fail to skew towards N2 phenotype. Flow cytometry analyzed the proportion of total neutrophils (CD11b+Ly-6G+) (**A**) and N2 phenotype neutrophils (Ly-6G+Arg1+) (**B**) in normal and diabetic wounds at day 1, 3, 5, and 7 (n=3). (**C**) Representative immunofluorescence images of Ly6G+pSTAT6+ neutrophils in wound sections from normal or diabetic mice. (**D**) Expressions of chemokine CCL2, CCL3, and CCL5 were examined by qRT-PCR. GAPDH was used as a normalization control (n=3). (**E**) Expressions of cytokines IL-4, IL-13, and IFN-gamma were examined by qRT-PCR. GAPDH was used as a normalization control (n=3). (**F**) In vivo distribution of CD31 labeled neovessels in wound sections from normal or diabetic mice. Scale bars, 100 μm. [*p < 0.05, **p < 0.01, ***p < 0.001, ****p < 0.0001; data were expressed as mean ± SD and analyzed by unpaired two-tailed *t*-test].

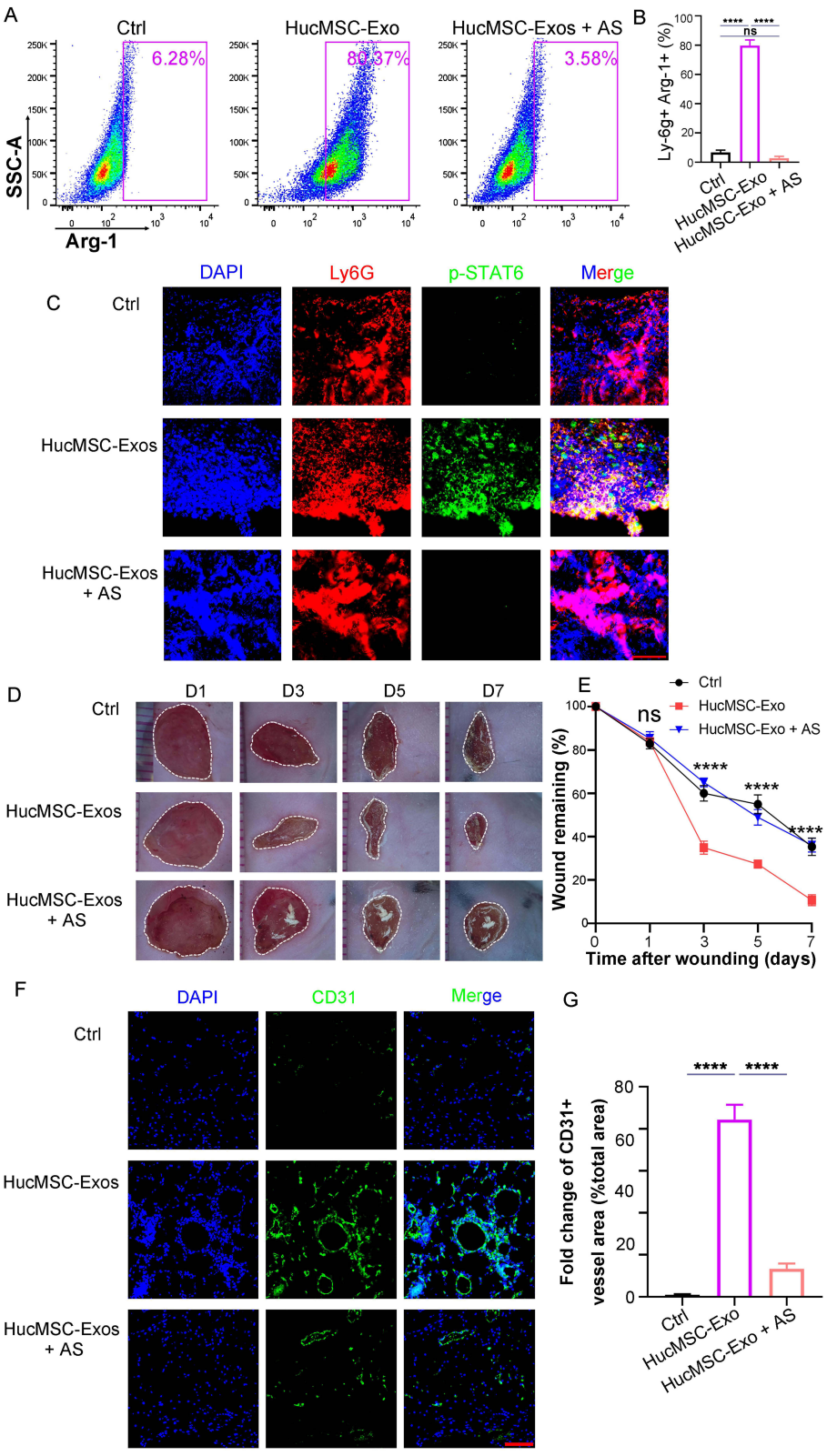

Figure 8 HucMSC-Exo facilitates angiogenesis and wound closure by inducing neutrophils skewing toward N2 phenotype in diabetic wounds. (**A**) Flow cytometry analyzed the proportion of N2 phenotype neutrophils (Ly-6G+Arg1+) in diabetic wounds treated with HucMSC-Exo or HucMSC-Exo plus AS1517499. (**B**) Quantitative analysis of the results in (**A**) (n=3). (**C**) Representative immunofluorescence images of Ly6G+pSTAT6+ neutrophils in wound treated with HucMSC-Exo or HucMSC-Exo plus AS1517499. Scale bars, 50 μm. (**D**) The gross view of wounds from mouse treated with HucMSC-Exo or HucMSC-Exo plus AS1517499. (**E**) Quantification of the wound closure. (**F**) In vivo distribution of CD31 labeled neovessels in wound treated with HucMSC-Exo or HucMSC-Exo plus AS1517499. Scale bars, 100 μm. (**G**) Quantification of fold change of CD31+ vessel area (% total area). [****p < 0.0001; data were expressed as mean ± SD and analyzed by unpaired two-tailed *t*-test].

https://doi.org/10.2147/IJN.S458295 DovePress

proved detrimental to the wound-healing process, aligning with previous observations.[8,10,36] Our prior findings provided evidence that HucMSC-Exo significantly ups the count of infiltrated neutrophils at the wound site in mice (930 vs 157, $p < 0.00001$).[16] These cells are paramount in early inflammation, serving as a frontline defense against microbes. However, emerging experimental evidences suggest that neutrophils possess alternative functions beyond their classic bactericidal roles.[37,38] In our present study, the administration of HucMSC-Exo failed to confer protection after depleting neutrophils, suggesting that neutrophils do not exert detrimental effects in the presence of HucMSC-Exo. Besides, it is highly conceivable that the pro-healing effect of HucMSC-Exo is contingent upon the presence of infiltrated neutrophils.

The unexpected association between the pro-healing effect induced by HucMSC-Exo and increased neutrophil numbers at wound sites prompted us to ponder over the existence of distinct neutrophil subsets with different pathophysiological roles. We speculated that HucMSC-Exo might reprogram neutrophils into a beneficial phenotype, much like the tissue-repairing M2 macrophage phenotype, which is recognized for tempering inflammation and facilitating tissue repair.[18,37,39–44] Cutting-edge research in oncology has revealed that neutrophils within tumor environments can manifest a pro-tumor N2 phenotype by expressing Arg1, CCL2, and CCL5, mainly regulated by the transforming growth factor-β within the tumor milieu.[45] Extending this concept to wound healing, we found a diverse array of neutrophils at the injury site, with a notable fraction expressing M2 markers— Arg1—marking the first reported occurrence of N2 neutrophils in skin tissue.

Interestingly, HucMSC-Exo have the potential to skew macrophages towards the M2 phenotype.[3] We hypothesized that similar phenotypic alterations occur in neutrophils, accounting for the improved healing despite increased density of neutrophils in wounds. Arg1 is widely recognized as a definitive indicator of M2 polarization in macrophages within mice and is also known to express under inflammatory conditions in the skin.[46] The presence of Arg1 has been linked with various healing processes including new blood vessel formation, wound closure, and reducing inflammation, with its skin expression closely tied to reparative outcomes.[46–48] We conducted a quantitative assessment of $Arg1^+$ (N2) neutrophilic subpopulations in the wound lesion and determine if HucMSC-Exo could affect their phenotypic balance. After the initial wound, our observations, taking place at 24 hours, showed that around one in three neutrophils in the wound region were Arg1-positive—a percentage that remained unchanged with HucMSC-Exo administration. Interestingly, at the 72-hour mark, a marked increase in Arg1-positive neutrophils was recorded in specimens that treated with HucMSC-Exo. It's important to note that these N2 neutrophils originated from local phenotype alterations at the wound site, as opposed to being a result of circulating N2 neutrophils' infiltration, which was substantiated by the lack of Arg1-positive neutrophils detected in the bloodstream following injury in mice that had received HucMSC-Exo treatment. Notably, deeper researches are warranted to discern if this Arg1+ population is homogeneous or consists of different neutrophilic subsets. Nevertheless, our findings provide the inaugural demonstration of HucMSC-Exo-driven reprogramming of neutrophils to an N2 phenotype, fostering their infiltration at wound sites in association with a healing outcome.

When exploring the molecular mechanisms behind this phenotype switching of N2 neutrophils following insult in the presence of HucMSC-Exo intervention, we observed an augmentation in the phosphorylation of STAT6 and upregulated expression of its transcriptional target, namely Arg1, pivotal in the immune-suppressive state of neutrophils. As a crucial mediator in the immunosuppressive programming of macrophages, STAT6 serves as a co-factor for PPARγ, facilitating the activation of gene transcription that regulates FAO metabolism.[30] As a result of these findings, we delved into the impact of phosphorylated STAT6 (p-STAT6) on the gene expression involved. Our discoveries revealed that blocking STAT6 significantly reduced the expression levels of PPARγ and FAO genes including *Cpt1b, Acadm, and Acadl*. During the polarization of macrophages, PPARγ collaborates with STAT6 to provoke lipid uptake and stimulate FAO activity, which serves as a primary energy source to satisfy the metabolic needs of M2 macrophages.[49] In neutrophils, we observed that HucMSC-Exo induced STAT6 signaling activation, leading to the upregulation of lipid uptake and FAO. Moreover, metabolic shifts that delineate the bioenergetic distinctions between N1 and N2 neutrophils are critical to their activation and functionality. N2 neutrophils, with their high energy demands, tap into mechanisms that enhance oxidative phosphorylation (OXPHOS) and lipid oxidation. In contrast, N1 neutrophils mainly depend on glycolysis, an ATP-producing pathway albeit a less efficient one. To encapsulate, our study uncovers a previously unidentified influence of HucMSC-Exo in modulating neutrophil phenotype shifts, guiding the function of STAT6-dependent FAO, and effectively dictating the energy state of N2 neutrophils.

While the role of neutrophils in healing has been debated—with high numbers often equated with detrimental inflammation[50,51] alternative perspectives suggest neutrophils go beyond their traditional bactericidal roles.[37] Previous studies have highlighted the importance of myeloid cells in adult neovascularization and angiogenesis. Notably, in contrast to macrophage depletion, the depletion of host neutrophils significantly impairs vasculogenesis in UGrafts, while adoptive transfer of neutrophils restores vascularization in myeloid-depleted mice.[27] Activated neutrophils can directly stimulate angiogenesis by releasing vascular endothelial growth factor (VEGF). Additionally, neutrophils can release BV8 to promote angiogenesis.[52] The presence of neutrophils has been associated with promoting angiogenesis, providing abundant oxygen and nutrients for cancer cell growth.[52] However, the impact of different neutrophil phenotypes on angiogenesis and tissue regeneration remains largely unknown. Our data strongly support the involvement of HucMSC-Exo in modulating myeloid cells after a wound insult. Importantly, we found that N2 neutrophils, alternatively activated by HucMSC-Exo in the wound, secreted more BV8. This secretion facilitated neovascularization and angiogenesis in a paracrine manner, representing a crucial step in wound healing. Interestingly, our findings revealed that the adoptive transfer of BV8-null neutrophils was less effective in inducing angiogenesis compared to wild-type neutrophils, suggesting BV8 represents a potential bone marrow-derived driver of angiogenesis.

Diabetic wounds are characterized by prolonged inflammation and poor angiogenesis. The chronic inflammatory state in diabetic individuals hinders the normal healing process, leading to delayed wound closure and increased risk of infections.[53] This persistent inflammation is often accompanied by an imbalance in pro-inflammatory and anti-inflammatory cytokines, impairing tissue repair and regeneration. In our research, we found a remarkable elevation in the levels of chemokines CCL2, CCL3, and CCL5, which are known to play a critical role in the recruitment and activation of neutrophils within the wound environment. These chemokines act as chemoattractants, guiding neutrophils to the site of injury and initiating the immune response. On the other hand, our investigation also revealed a notable decline in the concentrations of IL-4 and IL-13, which are important cytokines involved in the polarization and programming of N2 neutrophils. This intricate immune dysregulation observed in diabetic wounds may partly explained why there are more neutrophils infiltrating to the wound but less N2 subtype in diabetic wounds.

Addressing the factors that contribute to poor angiogenesis in diabetic wounds is essential for effective wound management.[34] The reduced blood supply and inadequate formation of new blood vessels limit nutrient and oxygen delivery to the wound site, hindering the formation of granulation tissue and impeding the healing process.[54] Our research highlights the proangiogenetic effects of HucMSC-Exo, which not only directly impact endothelial cells but also indirectly by modulating neutrophil polarization towards the N2 phenotype. It demonstrates a previously unexplored pathway of HucMSC-Exo action that could be pivotal for therapeutic interventions in diabetic wound care. Notably, it also uncovers a potential target, p-STAT6, in boosting the healing process, offering insight for future drug development.

In a nutshell, our data provided preliminary evidences that metabolic reprogramming induced by HucMSC-Exo plays a crucial role in modulating neutrophil behavior after wound induction. We presents a groundbreaking revelation that M2-like, N2 neutrophils exist within skin wound sites. The ability of HucMSC-Exo to modulate neutrophil polarization at these sites introduces an innovative pathway for controlling acute inflammatory responses, and further, shines a light on a novel mechanism through which wound healing can be markedly enhanced. This discovery holds considerable significance in regenerative medicine, highlighting HucMSC-Exo's therapeutic potential for advancing tissue repair and regeneration. Moreover, HucMSC-Exo's capacity to steer neutrophil polarization toward the N2 phenotype deepens our insight into the intricate crosstalk between immune responses and angiogenic pathways, paving the way for innovative treatments that target these processes for improved wound healing and tissue restoration.

Ethics Approval and Consent to Participate

All animal experiments confirmed to the Institutional Review Board of Chinese PLA General hospital [Number: 2023-144].

Author Contributions

All authors made a significant contribution to the work reported, whether that is in the conception, study design, execution, acquisition of data, analysis and interpretation, or in all these areas; took part in drafting, revising or critically reviewing the article; gave final approval of the version to be published; have agreed on the journal to which the article has been submitted; and agree to be accountable for all aspects of the work.

Disclosure

All authors declare no conflicts of interest in this work.

References

1. Yang J, Chen Z, Pan D, Li H, Shen J. Umbilical Cord-Derived Mesenchymal Stem Cell-Derived Exosomes Combined Pluronic F127 Hydrogel Promote Chronic Diabetic Wound Healing and Complete Skin Regeneration. *Int J Nanomed*. 2020;15:5911–5926. doi:10.2147/IJN.S249129
2. Li Q, Gong S, Yao W, et al. Exosome loaded genipin crosslinked hydrogel facilitates full thickness cutaneous wound healing in rat animal model. *Drug Deliv*. 2021;28(1):884–893. doi:10.1080/10717544.2021.1912210
3. Teng L, Maqsood M, Zhu M, et al. Exosomes Derived from Human Umbilical Cord Mesenchymal Stem Cells Accelerate Diabetic Wound Healing via Promoting M2 Macrophage Polarization, Angiogenesis, and Collagen Deposition. *Int J Mol Sci*. 2022;23(18):10421. doi:10.3390/ijms231810421
4. Rani S, Ritter T. The Exosome - A Naturally Secreted Nanoparticle and its Application to Wound Healing. *Adv Mater*. 2016;28(27):5542–5552. doi:10.1002/adma.201504009
5. Qin X, He J, Wang X, Wang J, Yang R, Chen X. The functions and clinical application potential of exosomes derived from mesenchymal stem cells on wound repair: a review of recent research advances. *Front Immunol*. 2023;14:1256687. doi:10.3389/fimmu.2023.1256687
6. Singer AJ, Clark RA. Cutaneous wound healing. *N Engl J Med*. 1999;341(10):738–746. doi:10.1056/NEJM199909023411006
7. Hwang J, Seo Y, Jeong D, et al. Monitoring Wound Healing with Topically Applied Optical NanoFlare mRNA Nanosensors. *Adv Sci (Weinh)*. 2022;9(18):e2104835. doi:10.1002/advs.202104835
8. Phillipson M, Kubes P. The Healing Power of Neutrophils. *Trends Immunol*. 2019;40(7):635–647. doi:10.1016/j.it.2019.05.001
9. Chu Z, Huang Q, Ma K, et al. Novel neutrophil extracellular trap-related mechanisms in diabetic wounds inspire a promising treatment strategy with hypoxia-challenged small extracellular vesicles. *Bioact Mater*. 2023;27:257–270. doi:10.1016/j.bioactmat.2023.04.007
10. Peiseler M, Kubes P. More friend than foe: the emerging role of neutrophils in tissue repair. *J Clin Invest*. 2019;129(7):2629–2639. doi:10.1172/JCI124616
11. Stremmel C, Stark K, Schulz C. Heterogeneity of Macrophages in Atherosclerosis. *Thromb Haemost*. 2019;119(8):1237–1246. doi:10.1055/s-0039-1692665
12. Vallejo J, Cochain C, Zernecke A, Ley K. Heterogeneity of immune cells in human atherosclerosis revealed by scRNA-Seq. *Cardiovasc Res*. 2021;117(13):2537–2543. doi:10.1093/cvr/cvab260
13. Dong T, Chen X, Xu H, et al. Mitochondrial metabolism mediated macrophage polarization in chronic lung diseases. *Pharmacol Ther*. 2022;239:108208. doi:10.1016/j.pharmthera.2022.108208
14. Locati M, Curtale G, Diversity MA. Mechanisms, and Significance of Macrophage Plasticity. *Annu Rev Pathol*. 2020;15(1):123–147. doi:10.1146/annurev-pathmechdis-012418-012718
15. Ng LG, Ostuni R, Hidalgo A. Heterogeneity of neutrophils. *Nat Rev Immunol*. 2019;19(4):255–265. doi:10.1038/s41577-019-0141-8
16. Liu Y, Zhang M, Liao Y, et al. Human umbilical cord mesenchymal stem cell-derived exosomes promote murine skin wound healing by neutrophil and macrophage modulations revealed by single-cell RNA sequencing. *Front Immunol*. 2023;14:1142088. doi:10.3389/fimmu.2023.1142088
17. Zhang W, Lin J, Shi P, et al. Small Extracellular Vesicles Derived From MSCs Have Immunomodulatory Effects to Enhance Delivery of ASO-210 for Psoriasis Treatment. *Front Cell Dev Biol*. 2022;10:842813. doi:10.3389/fcell.2022.842813
18. Yan X, Anzai A, Katsumata Y, et al. Temporal dynamics of cardiac immune cell accumulation following acute myocardial infarction. *J Mol Cell Cardiol*. 2013;62:24–35. doi:10.1016/j.yjmcc.2013.04.023
19. Ohms M, Möller S, Laskay T. An Attempt to Polarize Human Neutrophils Toward N1 and N2 Phenotypes in vitro. *Front Immunol*. 2020;11:532. doi:10.3389/fimmu.2020.00532
20. Mihaila AC, Ciortan L, Macarie RD, et al. Transcriptional Profiling and Functional Analysis of N1/N2 Neutrophils Reveal an Immunomodulatory Effect of S100A9-Blockade on the Pro-Inflammatory N1 Subpopulation. *Front Immunol*. 2021;12:708770. doi:10.3389/fimmu.2021.708770
21. Grunewald M, Avraham I, Dor Y, et al. VEGF-induced adult neovascularization: recruitment, retention, and role of accessory cells. *Cell*. 2006;124(1):175–189. doi:10.1016/j.cell.2005.10.036
22. Nahrendorf M, Swirski FK, Aikawa E, et al. The healing myocardium sequentially mobilizes two monocyte subsets with divergent and complementary functions. *J Exp Med*. 2007;204(12):3037–3047. doi:10.1084/jem.20070885
23. Shojaei F, Zhong C, Wu X, Yu L, Ferrara N. Role of myeloid cells in tumor angiogenesis and growth. *Trends Cell Biol*. 2008;18(8):372–378. doi:10.1016/j.tcb.2008.06.003
24. Revelo XS, Parthiban P, Chen C, et al. Cardiac Resident Macrophages Prevent Fibrosis and Stimulate Angiogenesis. *Circ Res*. 2021;129(12):1086–1101. doi:10.1161/CIRCRESAHA.121.319737
25. Du S, Qian J, Tan S, et al. Tumor cell-derived exosomes deliver TIE2 protein to macrophages to promote angiogenesis in cervical cancer. *Cancer Lett*. 2022;529:168–179. doi:10.1016/j.canlet.2022.01.005
26. Qiu S, Xie L, Lu C, et al. Gastric cancer-derived exosomal miR-519a-3p promotes liver metastasis by inducing intrahepatic M2-like macrophage-mediated angiogenesis. *J Exp Clin Cancer Res*. 2022;41(1):296. doi:10.1186/s13046-022-02499-8
27. Lin RZ, Lee CN, Moreno-Luna R, et al. Host non-inflammatory neutrophils mediate the engraftment of bioengineered vascular networks. *Nat Biomed Eng*. 2017;1.

28. Xing X, Bai Y, Song J. The Heterogeneity of Neutrophil Recruitment in the Tumor Microenvironment and the Formation of Premetastatic Niches. *J Immunol Res*. 2021;2021:6687474. doi:10.1155/2021/6687474
29. Li C, Xu X, Wei S, Jiang P, Xue L, Wang J. Tumor-associated macrophages: potential therapeutic strategies and future prospects in cancer. *J Immunother Cancer*. 2021;9(1):e001341. doi:10.1136/jitc-2020-001341
30. Hinshaw DC, Hanna A, Lama-Sherpa T, et al. Hedgehog Signaling Regulates Metabolism and Polarization of Mammary Tumor-Associated Macrophages. *Cancer Res*. 2021;81(21):5425–5437. doi:10.1158/0008-5472.CAN-20-1723
31. Varga T, Mounier R, Horvath A, et al. Highly Dynamic Transcriptional Signature of Distinct Macrophage Subsets during Sterile Inflammation, Resolution, and Tissue Repair. *J Immunol*. 2016;196(11):4771–4782. doi:10.4049/jimmunol.1502490
32. Iribarne M. Inflammation induces zebrafish regeneration. *Neural Regen Res*. 2021;16(9):1693–1701. doi:10.4103/1673-5374.306059
33. Kim MK, Kim Y, Park S, et al. Effects of Steady Low-Intensity Exercise on High-Fat Diet Stimulated Breast Cancer Progression Via the Alteration of Macrophage Polarization. *Integr Cancer Ther*. 2020;19:1534735420949678. doi:10.1177/1534735420949678
34. Huang F, Lu X, Yang Y. Microenvironment-Based Diabetic Foot Ulcer Nanomedicine. *Adv Sci* 2023;10(2):e2203308. doi:10.1002/advs.202203308
35. Hu Y, Rao SS, Wang ZX, et al. Exosomes from human umbilical cord blood accelerate cutaneous wound healing through miR-21-3p-mediated promotion of angiogenesis and fibroblast function. *Theranostics*. 2018;8(1):169. doi:10.7150/thno.21234
36. Wilgus TA, Roy S, McDaniel JC. Neutrophils and Wound Repair: positive Actions and Negative Reactions. *Adv Wound Care*. 2013;2(7):379–388. doi:10.1089/wound.2012.0383
37. Wang J, Hossain M, Thanabalasuriar A, Gunzer M, Meininger C, Kubes P. Visualizing the function and fate of neutrophils in sterile injury and repair. *Science*. 2017;358(6359):111–116. doi:10.1126/science.aam9690
38. Fischer A, Wannemacher J, Christ S, et al. Neutrophils direct preexisting matrix to initiate repair in damaged tissues. *Nat Immunol*. 2022;23 (4):518–531. doi:10.1038/s41590-022-01166-6
39. Cuartero MI, Ballesteros I, Moraga A, et al. N2 neutrophils, novel players in brain inflammation after stroke: modulation by the PPARγ agonist rosiglitazone. *Stroke*. 2013;44(12):3498–3508. doi:10.1161/STROKEAHA.113.002470
40. García-Culebras A, Durán-Laforet V, Peña-Martínez C, et al. Role of TLR4 (Toll-Like Receptor 4) in N1/N2 Neutrophil Programming After Stroke. *Stroke*. 2019;50(10):2922–2932. doi:10.1161/STROKEAHA.119.025085
41. Hou Y, Yang D, Xiang R, et al. N2 neutrophils may participate in spontaneous recovery after transient cerebral ischemia by inhibiting ischemic neuron injury in rats. *Int Immunopharmacol*. 2019;77:105970. doi:10.1016/j.intimp.2019.105970
42. Nederlof R, Reidel S, Spychala A, et al. Insulin-Like Growth Factor 1 Attenuates the Pro-Inflammatory Phenotype of Neutrophils in Myocardial Infarction. *Front Immunol*. 2022;13:908023. doi:10.3389/fimmu.2022.908023
43. Jiayi Mao LC, Zhengwei Cai SQ, Zhimo Liu BZ, Yuguang Zhang XS, Cui W. Advanced Biomaterials for Regulating Polarization of Macrophages in Wound Healing. *Adv Funct Mater* 2022. 32(12):202111003.
44. Jiayi Mao ZC, Zhimo Liu SQ, Binfan Zhao YZ, Yaping Zhuang LZ, Xiyuan Mao YZ, Wenguo Cui XS. Charge and receptor functional injectable hydrogels as cytokine-releasing reservoirs for wound healing. *Chem Eng J*. 2022;450:137880.
45. Fridlender ZG, Sun J, Kim S, et al. Polarization of tumor-associated neutrophil phenotype by TGF-beta: "N1" versus "N2" TAN. *Cancer Cell*. 2009;16(3):183–194. doi:10.1016/j.ccr.2009.06.017
46. Villarreal-Ponce A, Tiruneh MW, Lee J, et al. Keratinocyte-Macrophage Crosstalk by the Nrf2/Ccl2/EGF Signaling Axis Orchestrates Tissue Repair. *Cell Rep*. 2020;33(8):108417. doi:10.1016/j.celrep.2020.108417
47. Yin Y, Hao H, Cheng Y, et al. Human umbilical cord-derived mesenchymal stem cells direct macrophage polarization to alleviate pancreatic islets dysfunction in type 2 diabetic mice. *Cell Death Dis*. 2018;9(7):760. doi:10.1038/s41419-018-0801-9
48. Mao J, Qian S, Zhao Q, et al. Balancing macrophage polarization via stem cell-derived apoptotic bodies for diabetic wound healing. *Med*. 2024;5 (2):148–168.e8. doi:10.1016/j.medj.2024.01.006
49. Chawla A. Control of macrophage activation and function by PPARs. *Circ Res*. 2010;106(10):1559–1569. doi:10.1161/CIRCRESAHA.110.216523
50. Denorme F, Portier I, Rustad JL, et al. Neutrophil extracellular traps regulate ischemic stroke brain injury. *J Clin Invest*. 2022;132(10). doi:10.1172/JCI154225.
51. Zhao Z, Pan Z, Zhang S, et al. Neutrophil extracellular traps: a novel target for the treatment of stroke. *Pharmacol Ther*. 2023;241:108328. doi:10.1016/j.pharmthera.2022.108328
52. Ozel I, Duerig I, Domnich M, Lang S, Pylaeva E, Jablonska J. The Good, the Bad, and the Ugly: neutrophils, Angiogenesis, and Cancer. *Cancers*. 2022;14(3):536. doi:10.3390/cancers14030536
53. Armstrong DG, Tan TW, Boulton A, Bus SA. Diabetic Foot Ulcers. *JAMA*. 2023;330(1):62. doi:10.1001/jama.2023.10578
54. Wang X, Li R, Zhao H. Enhancing angiogenesis: innovative drug delivery systems to facilitate diabetic wound healing. *Biomed. Pharmacother.* 2023;170:116035. doi:10.1016/j.biopha.2023.116035